EurJIC
European Journal of Inorganic Chemistry

A Journal of ChemPubSoc Europe

Accepted Article

Title: Surface Defects as a Tool to Solubilize and Functionalize WS2 Nanotubes

Authors: Wolfgang Tremel, Dmitri Spetter, Faegheh Hoshyargar, Jugal Sahoo, Muhammad Nawaz Tahir, Robert Branscheid, Bastian Barton, Martin Panthöfer, and Ute Kolb

To be cited as: *Eur. J. Inorg. Chem.* 10.1002/ejic.201601361

Link to VoR: http://dx.doi.org/10.1002/ejic.201601361

WILEY-VCH

Surface Defects as a Tool to Solubilize and Functionalize WS_2 Nanotubes

Dmitri Spetter, Faegheh Hoshyargar, Jugal Kishore Sahoo, Muhammad Nawaz Tahir, Robert Branscheid, Bastian Barton, Martin Panthöfer, Ute Kolb, Wolfgang Tremel*

Dedication ((optional))

Layered transition metal dichalcogenides contain a number of crystal defects which significantly change their properties may be beneficial or detrimental for a specific application. We have prepared defect-rich multiwalled WS_2 nanotubes by reductive sulfidization of $W_{18}O_{49}$ nanowires that were obtained solvothermally from tungsten chloride in different alcohols. The synthesis of the $W_{18}O_{49}$ nanowires was monitored and their morphological characteristics (e. g. length, rigidity and aspect ratio) are described in detail. The effect of morphology of the nanowires on the synthesis of WS_2 nanotubes was investigated in order to obtain WS_2 nanotubes that are highly solvent dispersible. Dispersions of the WS_2 nanotubes in organic solvents were very stable for several days. The nanotubes could easily be functionalized with noble metals, metal oxides and Janus-type metal@metal oxide nanoparticles. The synthesis of nano-wires and nanotubes and the immobilization of the nanoparticles is demonstrated by transmission electron microscopy (TEM), high resolution transmission electron microscopy (HRTEM) combined with energy dispersive X-ray spectroscopy (EDX), electron diffraction, X-ray diffraction (XRD) and Raman spectroscopy.

Introduction

Transition metal dichalcogenides (TMCs) are in the focus of interest because of their exotic properties and many possible applications.[1-7] Ultrathin two-dimensional nanosheets of layered TMCs, nanotubes (NTs) or nested inorganic fullerenes (IFs) are allotropes of layered TMCs at the nanoscale[8-12] that have demonstrated great potential for applications in solid lubrication,[2,13-18] as cathode materials in rechargeable batteries,[19,20] as shock-resistant materials,[21,22] in sulfur removal catalysis and hydrogen evolution reactions.[23-27] Many properties of these nanomaterials such as tribological behavior, mechanical strength, electrical resistivity or optical and magnetic properties are related to their crystal structure, which is characterized by weak van der Waals forces between the MQ_2 layers, which contain metal atoms (M) sandwiched between two chalcogen layers (Q).[28] TMCs contain defects that can significantly affect their mechanical strength, ionic or electronic transport, and other physical properties. The surface curvature in nanotubes and nested fullerenes induces elastic strain that requires the insertion of new topological elements or defects to alleviate the strain induced by folding.[23]

Institute of Inorganic Chemistry and Analytical Chemistry, Johannes Guten berg University,
Duesbergweg 10-14, D-55128 Mainz, Germany
tremel@uni-mainz.de

Supporting information for this article is given via a link at the end of the document.

Defects moderate the chemical potential and affect the reactivity. Discrepancies between experiment and theory require TMCs – similar as carbon – to be viewed as real materials with defects rather than an infinitely large layered materials with perfect periodicity.[24,25] Defects residing in the MQ_2 layers may be classified as 0-D (point defects, impurities, non-hexagonal rings), 1-D (edges, grain boundaries), or 2D (stacking faults, solding etc.) which can arise as a result of thermal equilibrium or the kinetics of processing. In order to exploit applications of TMC nanostructures it is essential to control their defect density and interface structure. Although the surfaces of TMC nanomaterials have been tailored in different ways, little is known concerning their surface and defect structure. It has been demonstrated that point defects on the surfaces of chalcogenide NTs can be identified as reactive sites with chalcophilic markers such as gold nanoparticles.[26-28] In contrast, silane coating of WS_2 NTs passivated point defects, and no binding of gold nanoparticles was observed. These findings suggest that a tailoring of layered metal chalcogenide surfaces requires surface defects and their functionalization density is proportional to the defect concentration. Therefore, there is a need to design synthetic methods which results in a maximum number of surface defects while still preserving the bulk characteristics.

WS_2 nanotubes have been prepared by a variety of methods, in general with the goal to obtain defect-free nanoparticles. Reductive sulfidization of WO_x nanoparticles has proven to be the most efficient method for the synthesis of WS_2 nanoparticles, either as inorganic fullerenes or nanotubes.[29-32] In addition, template-assisted self-assembly,[33] electron beam irradiation,[34] arc discharge,[35-37] and laser ablation[38] have been employed. In this contribution we show that the structure of the metal oxide precursors has an effect on the defect density of WS_2 nanoparticles obtained by reductive sulfidization. Heavily defected WS_2 nanotubes were obtained by sulfidization of $W_{18}O_{49}$ nanowires that were prepared by solvolysis of WCl_6 in different alcohols under solvothermal conditions or by hot injection. The as-synthesized nanowires with high defect levels had diameters between 10-40 nm and lengths ranging from several hundreds of nanometer to few micrometers. The effect of the precursor morphology on the crystallinity, defect density and dispersibility of the NTs was studied. Defect-rich nanotubes could massively be functionalized with different types of metal nanoparticles.

Results and Discussion

$W_{18}O_{49}$ nanowires were prepared by solvothermal treatment of WCl_6 and sulfidized subsequently with H_2S to obtain WS_2 nanotubes. Figure 1 illustrates the synthetic route for the

preparation of the $W_{18}O_{49}$ nanowires and their conversion to WS_2 nanotubes. In the first step, a tungsten chloride solution in ethanol was diluted with an alcohol (ROH, R = Me, Et, Pr and c-C_6H_{11}) and transferred into a Teflon-lined vessel which was sealed in a stainless steel autoclave and subjected to a solvothermal treatment. After cooling to room temperature dark blue nanowires of $W_{18}O_{49}$ were obtained. In a second reaction step the $W_{18}O_{49}$ nanowires were used as precursor to synthesize WS_2 nanotube by reaction with H_2S for 30 min at 850°C.

The as-synthesized nanowires and the resulting WS_2 nanotubes were characterized by TEM and HRTEM. Figure 2 shows an overview of TEM and high resolution (HR-TEM) images of the $W_{18}O_{49}$ nanowires obtained from methanol (Figures 2a and d), ethanol (Figures 2b and e), and propanol (Figures 2c and f).

The diameter and length of the nanowires could be tuned from 10-40 nm and 1-10 μm, respectively, by changing the solvent (methanol to propanol). Nanowires obtained from propanol were uniform in diameter compared to those obtained from methanol or ethanol. The corresponding HRTEM images (Figures 2d-f) confirm a growth along the [010] direction (indicated by the arrow).

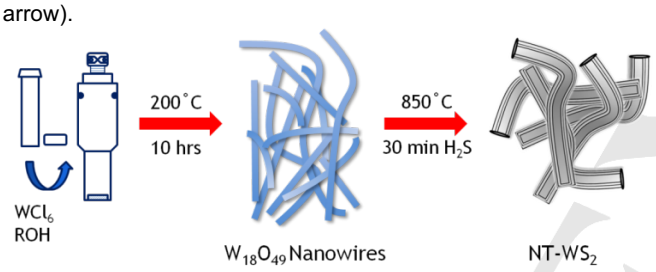

Figure 1. Formation of $W_{18}O_{49}$ nanowires and their transformation to WS_2 nanotubes.

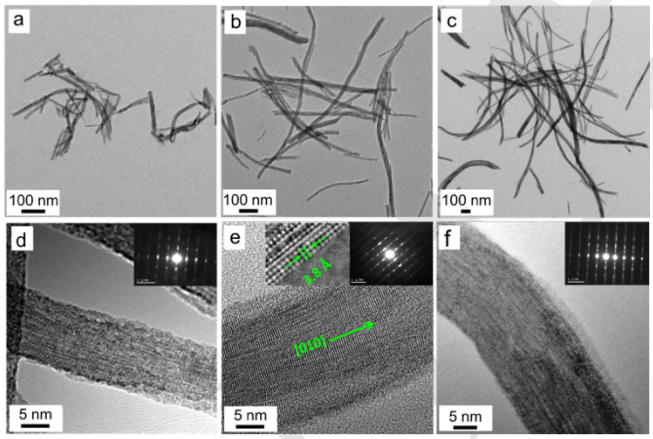

Figure 2. TEM overview (a-c) and HRTEM images (d-f) of $W_{18}O_{49}$ nanowires obtained from (a) methanol, (b) ethanol and (c) propanol solution. The insets (d-f) to show the ED patterns.

The Raman spectrum of the $W_{18}O_{49}$ nanowires reveals four main signals. The bands at 806 cm^{-1} and 695 cm^{-1} belong to W-O stretching modes, while 256 cm^{-1} and 187 cm^{-1} belong to O-W-O bending modes.[39] The bands at 806 cm^{-1} and 695 cm^{-1}, in particular, are broad because of a wide range of W-O-W bond lengths in the $W_{18}O_{49}$ structure. That can be attributed to the fact that the sub-oxides of tungsten (WO_x) are of an oxygen deficient type, which results in a mixture of different oxidation states of the tungsten atoms ranging from W^{4+} to W^{6+}.[40-43]

The results of HR-TEM, XRD and Raman spectroscopy (Figure 3) confirm that the samples obtained by solvothermal synthesis are single phase monoclinic $W_{18}O_{49}$. All as-synthesized nanowires synthesized in different alcohols exhibited the same phase ($W_{18}O_{49}$) based on XRD and Raman spectroscopy. Therefore, we present only a diffractogram and Raman spectrum of one representative product.

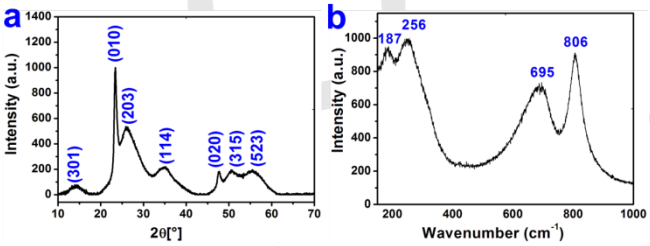

Figure 3. (a) X-ray powder diffraction pattern and (b) Raman spectra of as-synthesized tungsten oxide nanowires using propanol as solvent. Both match with the diffractogram and the Raman spectrum of $W_{18}O_{49}$.

Figure 4 shows TEM overview and HRTEM images of the WS_2 nanotubes. The morphology and %yield of the WS_2 nanotubes obtained from the $W_{18}O_{49}$ nanowires synthesized in propanol (Figure 4c) was much better than for nanotubes synthesized from $W_{18}O_{49}$ nanowires obtained in ethanol (Figure 2b, e) and methanol (Figure 2a, b).

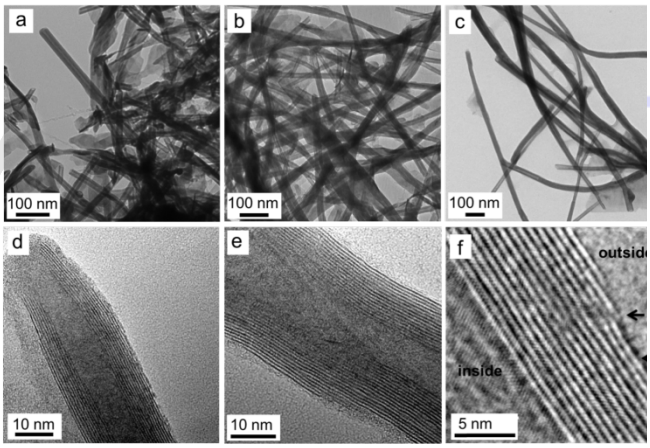

Figure 4. (a-c) TEM overview and corresponding (d-f) HRTEM images of WS_2 nanotubes obtained by sulfidization of $W_{18}O_{49}$ nanowires synthesized in (a, d) methanol, (b, e) ethanol and (c, f) propanol.

HRTEM revealed the presence of numerous defects on the outer surface of the nanotubes. One of the representative HRTEM image (Figure 4f) shows defects on the outer side (marked with arrows) while the inner surface is quite regular. Long (up to 4 μm), uniform and flexible WS_2 nanotubes were obtained from $W_{18}O_{49}$ nanowires synthesized in propanol with a conversion yield of ~100% (Figure 4c and Figure S3). Some morphological details of WS_2 nanotubes made from $W_{18}O_{49}$ nanowires obtained under different con-

ditions are summarized in Table S2. The X-ray diffractogram in Figure S1 shows the presence of single-phase 2H-WS_2 (PDF-2 file card No. 08-0237). However, on comparing the XRD pattern with WS_2 nanotubes reported by Houben et al. there might be also some stacking defects in the layers which could be attributed to 3R phase of WS_2.[44]
From a mechanistic point of view, the sulfidization can be assumed to start at the outer surface of the $W_{18}O_{49}$ nanowires. The defects are detected from the precursor nanowire (see Figure S4). WS_2 nanotubes obtained from $W_{18}O_{49}$ nanowires made in ethanol and propanol showed a Moiré-like pattern-like structure (Figure 4b, c). The HRTEM image of the closed-tip nanotube (Figure 5b) revealed a hexagonal dot lattice inside the nanotube. These graphene-type sheets (viewed edge-on) in the walls appear as dotted lines in Figure 5b and lead to a complex Moiré pattern similar to those observed in chiral multiwalled carbon nanotubes (MWCNTs).[43]

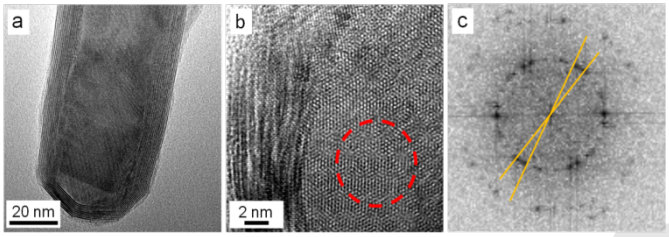

Figure 5. (a) TEM overview image of a closed-tip WS_2 nanotube showing the Moiré-like dot pattern in its central part. (b) HRTEM image of the WS_2 nanotube. (c) FFT of the area highlighted by the dashed red circle in (b).

Fast Fourier transform (FFT) of the selected area (Figure 5) shows a doublet pattern with three rings (corresponding to *d* values of 2.76 Å, 1.64 Å and 1.4 Å) resulting from the (100), (106) and (114) planes of 2H-WS_2, respectively. The presence of the Moiré-like pattern for the fully sulfidized WS_2 sheets shows the polychirality of the multi-walled WS_2 nanotubes. It is worth to mention that $W_{18}O_{49}$ nanowires get fully sulfidized in 30 min and to the best of our analysis; we did not observe any remaining oxide in the core of nanotubes. We have also sulfidized $W_{18}O_{49}$ nanorods obtained by hot injection.[45] However, all attempts to convert these $W_{18}O_{49}$ nanorods to WS_2 nanotubes were unsuccessful (only a 1-2% yield of WS_2 nanotubes was obtained (Figure S5)).

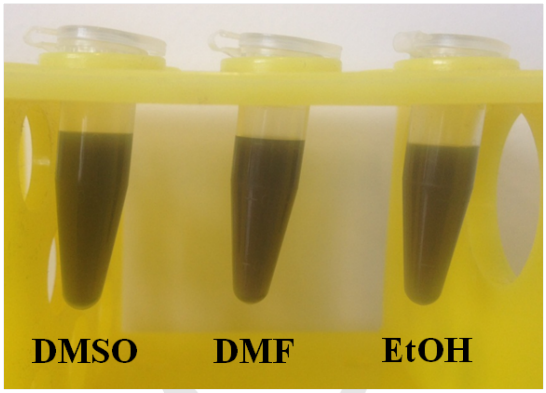

Figure 6. (a) Digital photograph showing the dispersibility of defect-rich WS_2 nanotubes in dimethylsulfoxide (DMSO), dimethylformamide (DMF) and ethanol (EtOH) and (c = 0.1 mg/mL).

Unlike WS_2 nanotubes derived from small WO_3 nanorods with an average length of 200 nm,[45] which can be solublized only after functionalization with chelating ligands,[46,47] defect-rich WS_2 nanotubes prepared from $W_{18}O_{49}$ nanowires (in this work) were soluble in a variety of solvents, and their suspensions were stable over time (Figure 6). These findings are in good agreement with a concept proposed by Tenne and co-workers that defects are more prone to adsorb water molecules which makes the chalcogenide particles highly soluble in polymeric solvents like DMF and DMSO. This phenomenon also explains the good dispersibility of the as-synthesized WS_2 nanotubes.
To demonstrate the concept of defect-rich nanotubes to achieve the high density of binding entities, as-synthesized nanotubes were reacted with different types of nanoparticles including metal, metal oxide and Janus type nanoparticles. In all cases, we achieved an almost full monolayer coverage, with nanoparticles on the side walls of the nanotubes (Figure 7). The overview TEM images (Figure 7a-c) confirmed almost all nanotubes to be uniformly coated with Pt@Fe_3O_4, MnO and Au nanoparticles, respectively. High resolution TEM images (Figure 7d-f) showed the binding of respective nanoparticles in a monolayer fashion. The high binding density of the nanoparticles suggests that defects-rich nanotubes not only improve properties like solubility but also allow to obtain hybrid nanocomposites. HRTEM images (Figure S6) depicts the chemisorption of nanoparticles onto the defects rich sidewalls of WS_2-nanotubes.

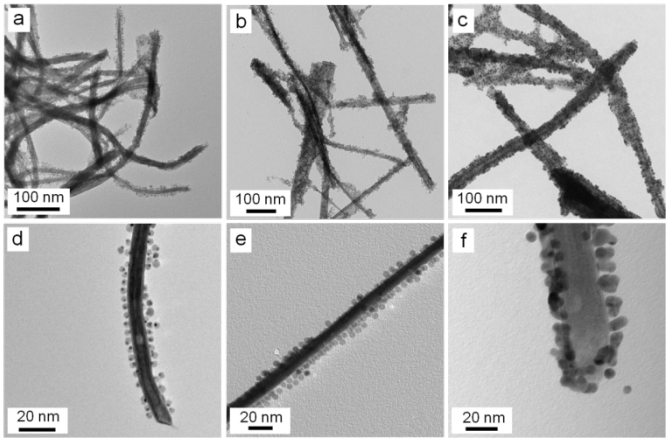

Figure 7. TEM images of WS_2 nanotubes covered with monolayers of (a, d) Pt@Fe_3O_4 Janus particles, (b, e) MnO nanoparticles and (c, f) Au nanoparticles.

Conclusion

We have demonstrated a facile synthesis of tungsten oxide nanowires. The changes their morphological characteristics (length, rigidity and aspect ratio) are described in detail. These nanowires were used as precursors for the synthesis of highly defective - and thus functionalizable - WS_2 nanotubes. Tungsten oxide nanowires synthesized in 1-propanol had the maximum number of dislocations. “Curved” and defective nanotubes were obtained after sulfidization. This allowed functionalization with noble metals, metal oxide and Janus-type metal@metal oxide nanoparticles.

Experimental Section

Solvothermal synthesis of $W_{18}O_{49}$ nanowires. The starting solution for all the experiments was prepared by dissolving 506.25 mg of tungsten hexachloride (98%, WCl_6, ABCR) in 25 mL of ethanol (P.A. VWR) by sonication ([WCl_6] = 0.05 M). Typically, the final solution was prepared by injecting 3.2 mL of the starting solution in a 50 mL Teflon-lined vessel containing 31.8 mL of the respective alcohol ([WCl_6] = 0.0045 M). The Teflon-lined vessel was sealed in a stainless steel autoclave. Unless mentioned otherwise, the solvothermal reaction was carried out for 10 h at 200 °C in an electric furnace. After the reaction, dark blue fluffy particles were collected by centrifugation, rinsed with ethanol three times and dried at 60 °C in vacuum. To study the influence of the concentration of the tungsten source on the morphology of the tungsten oxide nanowires, the final solution was also prepared in different concentrations (0.007 M and 0.0055 M) by injecting 5 mL and 3.9 mL of the starting solution into the Teflon-lined vessel containing 30 mL and 31.1 mL ethanol, respectively. To study the role of the alcohol on the growth and morphology of the tungsten oxide nanowires the reaction was carried out with methanol (≥99.8%, Sigma-Aldrich), 1-propanol (≥99.5%, Sigma-Aldrich) and cyclohexanol (99%, ABCR) in an analogous manner, and the final solution was in turn prepared by injection of 3.2 mL of the starting solution into the Teflon-lined vessel containing 31.8 mL of the alcohols.

Synthesis of $W_{18}O_{49}$ nanorods by hot injection. In a typical synthesis tungsten ethoxide (0.5 mL) was injected into a pre-heated solution of a mixture containing trioctyl amine (17.5 mL) and oleic acid (12.5 mL) at 320 °C. The temperature was held for 5 min, followed by cooling to room temperature. The $W_{18}O_{49}$ nanorods were precipitated by addition of 15 mL of ethanol. The product was collected by centrifugation and washed with ethanol and acetone.

Synthesis of WS_2 nantubes by reductive sulfidization of $W_{18}O_{49}$ nanorods/nanowires. The as-synthesized $W_{18}O_{49}$ nanowires/rods were placed in a corundum boat and kept inside a quartz tube which was flushed with argon for half an hour prior to the reaction to remove oxygen. The corundum boat was kept in the middle of the furnace and heated to 850 °C at the rate of 5 °C/min under a constant flow of argon. Just before reaching to 850 °C, the argon was switched to H_2S gas with a flow rate of 40 sccm and kept at this temperature for half an hour. The H_2S flow was carefully controlled using a flowmeter. After half an hour, the furnace was cooled to ambient temperature at the rate of 5 °C/min under constant flow of argon. The resulting black powder was collected and used for the further characterization.

Synthesis and immobilization of metal (Au), metal oxide (MnO) and Janus type metal@metal oxide (Pt@Fe_3O_4) nanoparticles onto WS_2 nanotubes.

Gold nanoparticles, MnO and Pt@Fe_3O_4 were synthesized as reported previously.[48-52] In a typical experiment 3 mg of WS_2 nanotubes were dispersed in 5 ml chloroform:ethanol (1:1) by sonicating the sample for 5-7 min. The solution was degassed under argon for 10-15 min. In another centrifuge vial, 8 mg of nanoparticles were dissolved in 5 ml of chloroform (Au, MnO, Pt@Fe_3O_4). Subsequently, the solution was added dropwise to the degassed mixture of WS_2 nanotubes over a period of 5-7 min. The reaction mixture was degassed again under argon for 5 min and put in a shaker for 2 h at room temperature (RT). After the reaction was complete, the unbound nanoparticles were washed out by centrifuging the sample three times at 4000 rpm for 10 min. Finally, the functionalized WS_2 nanocomposites were characterized by TEM/HRTEM combined with EDX. Samples for TEM were prepared by putting 1-2 drops of dispersed sample on a copper TEM grid followed by drying.

Materials characterization. X-ray diffraction patterns (XRD) were recorded on a Siemens D5000 diffractometer equipped with a Braun M50 position sensitive detector in transmission mode using Ge (200) monochromatized CuKα radiation. Samples were prepared between two layers of Scotch Magic Tape. Crystalline phases were identified according to the PDF–2 database using the Bruker AXS EVA 10.0 software.

Transmission electron microscopy (TEM) and electron diffraction (ED) were performed on a Phillips EM-420 equipped with a slow scan CCD detector (1k x 1k) and a LaB6 electron gun operated with an acceleration voltage of 120 kV. TEM images were processed with the Gnu Image Manipulation Program GIMP Version 2.6.8 or with Image J Version 1.43u. High resolution (HR) images were taken with a Philips FEI TECNAI F30 ST electron microscope (field-emission gun, 300 kV extraction voltages) equipped with an Oxford EDX (energy-dispersive X-ray) spectrometer with a Si/Li detector and an ultrathin window for elemental analysis and a STEM detector. TEM samples were prepared by dispersing the sample in ethanol and drop casting on 300 mesh carbon coated copper grids.

Raman spectra were recorded with a Horiba Yvon Lab RAM HR 800 spectrometer equipped with a microscope (Olympus BX41) and a CCD detector. The entrance slit was set to 100 µm, the laser focal spot was 2 x 2 µm. A Nd:YAG laser (532.12 nm) with a laser power 2 mW was used for excitation. The laser light was focused onto the fine powder sample using a 50x long working distance objective. All Raman spectra were recorded in backscattering geometry at a resolution of 0.5 cm^{-1} in the range between 150 and 1000 cm^{-1}, wherein at least 5 spectra for each sample where measured to improve the statistics.

Acknowledgements

We acknowledge support for the Electron Microscopy Center in Mainz (EZMZ) from the Center for INnovative and Emerging MAterials (CINEMA).

Keywords: Tungsten disulfide, nanotube, functionalization, defect

[1] J. Wilson and A. Yoffe, *Adv. Phys*. **1969**, *18*, 193−335.
[2] F. Hulliger, Structural Chemistry of the Layer-Type Phases (Ed.: F. Levy), Reidel, Dordrecht, 1976.
[3] D. Jariwala, V. K. Sangwan, L. J. Lauhon, T. J. Marks and M. C Hersam, *ACS Nano* **2014**, *8*, 1102−1120.
[4] M. F. Khan, M. W. Iqbal, M. Z. Iqbal, M. A. Shehzad, Y. Seo and J. Eom, *ACS Appl. Mater. Interfaces* **2014**, *6*, 21645−21651.
[5] M. Pumera, Z. Sofer and A. Ambrosi, *J. Mater. Chem. A* **2014**, *2*, 8981−8987.
[6] G. Xu, J. Wang, B. Yan and X.-L. Qi, *Phys. Rev. B: Condens. Matter Mater. Phys.* **2014**, *90*, 100505(R).
[7] D. Lembke, S. Bertolazzi and A. Kis, *Acc. Chem. Res*. **2015**, *48*, 100−110.
[8] A. Nag, K. Raidongia, K. P. S. S. Hembram, R. Datta, U. V. Waghmare, and C. N. R. Rao, *ACS Nano*, **2010**, *4*, 1539.
[9] K. S. Novoselov, D. Jiang, F. Schedin, T. J. Booth, V. V. Khotkevich, S. V. Morozov, and A. K. Geim, *Proc. Natl. Acad. Sci. USA,* **2005**, *102*, 10451.
[10] D. Yang and R. F. Frindt, *J. Phys. Chem. Solids,* **1996**, *57*, 1113.
[11] F. Hoshyargar, J. K. Sahoo, M. N. Tahir, A. Yella, M. Dietzsch, F. Natalio, R. Branscheid, U. Kolb, M. Panthöfer, and W. Tremel, *Dalton Trans.,* **2013**, *42*, 5292.
[12] M. Chhowalla, H. S. Shin, G. Eda, L.-J. Li, K. P. Loh, and H. Zhang, *Nat. Chem.,* **2013**, *5*, 263.
[13] A. Katz, M. Redlich, L. Rapoport, H. D. Wagner, and R. Tenne, *Tribol. Lett.,* **2006**, *21*, 135.
[14] J. Tannous, F. Dassenoy, B. Vacher, T. Le Mogne, A. Bruhacs, and W. Tremel, *Tribol. Lett.,* **2011**, *41*, 55.
[15] C. Lee, Q. Li, W. Kalb, X. Z. Liu, H. Berger, R. W. Carpick, and J. Hone, *Science*, **2010**, *328*, 76.
[16] I. Lahouij, E.W. Bucholz, B. Vacher, S.B. Sinnott, J.M. Martin, and F. Dassenoy, *Nanotechnology*, **2012**, *23*, 375701.
[17] J. Kogovšek and M. Kalin, *Tribol. Lett*., **2014**, *53*, 585.
[18] R. Greenberg, G. Halperin, I. Etsion, and R. Tenne, *Tribol. Lett*., **2004**, *17*, 179.
[19] S. J. Ding, D. Y. Zhang, J. S. Chen, and X. W. Lou, *Nanoscale*, **2012**, *4*, 95.
[20] Y. Q. Zhu, T. Sekine, Y. H. Li, W. X. Wang, M. W. Fay, H. Edwards, P. D. Brown, N. Fleischer, and R. Tenne, *Adv. Mater*., **2005**, *17*, 1500.
[21] J. Jang, S. Jeong, B. Park, J. Seo, J. Cheon, M.-C. Kim, E. Sim, Y. Oh, and S. Nam, *J. Am. Chem. Soc.,* **2011**, *133*, 7636.
[22] Y. Q. Zhu, T. Sekine, K. S. Brigatti, S. Firth, R. Tenne, R. Rosentsveig, H. W. Kroto, and D. R. M. Walton, *J. Am. Chem. Soc.,* **2003**, *125*, 1329.
[23] G. Z. Shen, Y. Bando, D. Golberg, and C. Zhou, *J. Phys. Chem. C,* **2008**, *112*, 5856.
[24] X. Zhou and B. I. Yakobson, *Acc. Chem. Res*. **2015**, *48*, 73.
[25] F. Banhart, J. Kotakowski and A. V. Krasheninnikov, *ACS Nano* **2011**, *6*, 26.
[26] A. R. Adini, M.Redlich, and R. Tenne, *J. Mater. Chem.,* **2011**, *21*, 15121.
[27] C. S. Reddy, A. Zak, and E. Zussman, *J. Mater. Chem.,* **2011**, *21,* 16086.
[28] C. Shahar, R. Levi, S. R. Cohen, and R. Tenne, J. *Phys. Chem. Lett.,* **2010**, *1*, 540.
[29] C. Shahar, D. Zbaida, L. Rapoport, H. Cohen, T. Bendikov, J. Tannous, F. Dassenoy, and R. Tenne, *Langmuir,* **2010**, *26*, 4409.
[30] A. Rothschild, J. Sloan, and R. Tenne, *J. Am. Chem. Soc.,* **2000**, *122*, 5169.
[31] H. A. Therese, J. Li, U. Kolb, and W. Tremel, *Solid State Sci.,* **2005**, *7*, 67.
[32] M. Remskar, M. Virsek, and A. Jesih, *Nano Lett.,* **2008**, *8*, 76.
[33] Y. D. Li, X. L. Li, R. R. He, J. Zhu, and Z. X. Deng, *J. Am. Chem. Soc.,* **2002**, *124,* 1411.
[34] M. J. Yacaman, H. Lopes, P. Santiago, D. H. Galvan, I. L. Garzon, and A. Reyes, *Appl. Phys. Lett.,* **1996**, *69*, 1065.
[35] I. Alexandrou, N. Sano, A. Burrows, R. R. Meyer, H. Wang, A. I. Kirkland, C. J. Kiely, and G. A. J. Amaratunga, *Nanotechnology,* **2003**, *14*, 913.
[36] J. J. Hu, J. E. Bultman, and J. S. Zabinski, *Tribol. Lett.,* **2004**, *17*, 543.
[37] V. Brüser, R. Popovitz-Biro, A. Albu-Yaron, T. Lorenz, G. Seifert, R. Tenne, and A. Zak, *Inorganics* **2014**, *2*, 177.
[38] R. Sen, A. Govindaraj, K. Suenaga, S. Suzuki, H. Kataura, S. Iijima, and Y. Achiba, *Chem. Phys. Lett.*, **2001**, *340*, 242.
[39] C. Guo, S. Yin, M. Yan, M. Kobayashi, M. Kakihana, and T. Sato, *Inorg. Chem.,* **2012**, *51*, 4763.
[40] M. Boulova, N. Rosman, P. Bouvier, and G. Lucazeau, *J. Phys.: Condens. Matter.,* **2002**, *14*, 5849.
[41] D. Y. Lu, J. Chen, J. Zhou, S. Z. Deng, N. S. Xu, and J. B. Xu, *J. Raman Spectrosc.,* **2007**, *38*, 176.
[42] C. Guo, S. Yin, M. Yan, M. Kobayashi, M. Kakihana, and T. Sato, *Inorg. Chem.*, **2012**, *51*, 4763.
[43] S. Amelinckx, A. Lucas, and P. Lambin, *Rep. Prog. Phys.,* 1999, **62,** 1471.
[44] L. Houben, A. N. Enyashin, Y. Feldman, R. Rosentsveig, D. G. Stroppa, M. Bar-Sadan, *J. Phys. Chem. C* **2012**, 116, 24350.
[45] A. Yella, M. N. Tahir, S. Meuer, R. Zentel, R. Berger, M. Panthöfer, and W. Tremel, *J. Amer. Chem. Soc.,* **2009**, *48*, 17566.
[46] J. K. Sahoo, M. N. Tahir, A. Yella, R. Branscheid, U. Kolb, and W. Tremel, *Langmuir,* **2011**, *27*, 385.
[47] M. N. Tahir, A. Yella, J. K. Sahoo, F. Natalio, U. Kolb, F. Jochum, P. Theato, and W. Tremel, *Isr. J. Chem.,* **2010**, *50*, 500.
[48] J. Küther, R. Seshadri, G. Nelles, H.-J. Butt, W. Assenmacher, W. Mader, and W. Tremel *Chem. Mater*. **1999**, *11*, 1317.
[49] T. D. Schladt, T. Graf, and W. Tremel *Chem. Mater.* **2009**, 21, 3183.
[50] J. K. Sahoo, M. N. Tahir, A. Yella, T. D. Schladt, E. Mugnaioli, U. Kolb. and W. Tremel, *Angew. Chem. Int. Ed.,* **2010**, *49*, 7578.
[51] T. D. Schladt, T. Graf, O. Köhler, H. Bauer, K. Schneider, C. Herold, J. Mertins, W. Tremel, *Chem. Mater.* **2012**, *24*, 525.
[52] J. K. Sahoo, M. N. Tahir, F. Hoshyargar, B. Nakhjavan, R. Branscheid, U. Kolb, W. Tremel, *Angew. Chem. Int. Ed.* **2011**, 50, 12271.

Entry for the Table of Contents

FULL PAPER

Defect-rich multiwalled WS_2 nanotubes were prepared by reductive sulfidization of $W_{18}O_{49}$ nanowires obtained by solvothermal synthesis from tungsten chloride in alcohols. The defect-rich WS_2 nanotubes were solvent dispersible and they could easily be functionalized with noble metals, metal oxides and Janus-type metal@metal oxide nanoparticles.

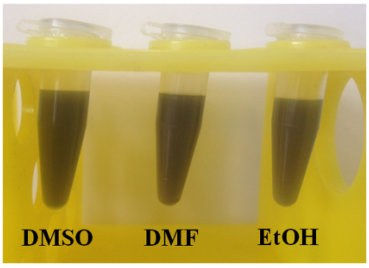

Chalcogenide nanotubes, functionalization

Dmitri Spetter, Faegheh Hoshyargar, Jugal Kishore Sahoo, Muhammad Nawaz Tahir, Robert Branscheid, Bastian Barton, Martin Panthöfer, Ute Kolb, Wolfgang Tremel

Page No. – Page No.

Surface Defects as a Tool to Solubilize and Functionalize WS_2 Nanotubes